Results in Engineering 24 (2024) 103150

Contents lists available at ScienceDirect

Results in Engineering

journal homepage: www.sciencedirect.com/journal/results-in-engineering

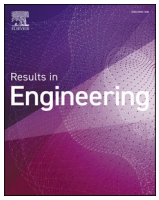

Unlocking the thermoelectric potential of nanocrystalline magnesium selenide thin films grown by single stage horizontal tube furnace (SSHTF)

Anas Al Tarabsheh [a,b], A. Rehman [c], K. Javaid [c], Lamia Ben Farhat [d], A. Ali [c], K. Mahmood [c,*], M. Yasir Ali [c], S. Ikram [c], Jolly Jacob [e]

[a] College of Engineering, Al Ain University, 112612, Abu Dhbi, United Arab Emirates
[b] Electrical Engineering Department, Faculty of Engineering, The Hashemite University, 13115, Zarqa, 330127, Jordan
[c] Department of Physics, Government College University Faisalabad, Pakistan
[d] Department of Chemistry, College of Sciences, King Khalid University, P.O. Box 9004, abha, Saudi Arabia
[e] College of Arts and Science, Abu Dhabi University, United Arab Emirates

ARTICLE INFO

Keywords:
MgSe thin films
Vacuum tube furnace
Source to substrate distance
Thermoelectric power generation

ABSTRACT

In this manuscript, the thin films of Magnesium Selenide (MgSe) were synthesized on a glass substrate using a single-stage horizontal tube furnace (SSHTF) which is supposed to be the simplest and a cost-effective approach. Before the deposition of thin films, the substrate was cleaned using standard methods. A pellet was formed by taking an equal ratio (1:1) of magnesium (Mg) and selenium (Se) powders and then evaporating them at 700°C for 1 h. The flow rate of nitrogen gas (100 SCCM) was maintained during the deposition process to avoid unwanted oxygen. A number of samples were synthesized by varying the source to substrate distance, and some representative samples are chosen for this study. The post-growth samples were characterized using XRD, SEM, and Raman Spectroscopy. The thermoelectric potential of all samples was tested by a home-developed Seebeck system. We have observed some promising values of the Seebeck coefficient (7.175×10^{-5} V/°C) and power factor (6.35×10^{-8} $Wm^{-1}{}^{o}C^{-2}$) at optimized source-to substrate distance. These encouraging results will open the door for MgSe-based thermoelectric research and further explore its power generation potential in the future.

1. Introduction

Conventional energy sources are limited, and soon, these sources will be expected to have vanished, so to meet the energy requirement, it is necessary to look for different alternative energy generation systems. These sources should produce green and environmentally friendly energy so that environment won't get affected [1,2]. There are different kinds of green and environmentally friendly energy production systems, such as hydro power, wind power, solar power, piezoelectric, and thermoelectric power generation system. Among them, thermoelectricity is one of the cheap and environment friendly source of energy because it harvests wasted heat energy from the environment and converts it into useable electrical energy [3–10]. It has been almost half a century since researchers are trying to improve the material's properties and making efforts to enhance the efficiency of thermoelectric power generation systems both in experimental and theoretical domains. The overall efficiency of material (both in power generation & refrigeration) is determined by a mathematical relation called (ZT) or figure of merit, which is dimensionless and given as (see Table 1)

$$ZT = S^2\sigma T/\kappa \quad (1)$$

Here in eq (1) Seebeck coefficient is represented by "S", and electrical conductivity is meant by "σ", whereas "κ" stands for thermal conductivity.

Although thermoelectric research has been a continuous point of interest for more than 50 years, the renaissance started in the 1990s. Hicks and his buddy researcher Dresselhaus published a research article in which they presented the idea of nanostructure's effect on material properties that brings new horizons in thermoelectric power generation. Two major pathways under the researcher's focus that help to enhance the Figure of merit (ZT) are reducing the thermal conductivity through the lattice. Low thermal conductivity could be achieved using different approaches, such as incorporating the rattler atom in the crystal structure. On the other hand, the 2nd approach is a significant improvement in the power factor, indicating better thermoelectric behavior. It

* Corresponding author.
E-mail address: khalid_mahmood856@yahoo.com (K. Mahmood).

https://doi.org/10.1016/j.rineng.2024.103150
Received 3 August 2024; Received in revised form 29 September 2024; Accepted 12 October 2024
Available online 14 October 2024

Table 1
The Xray diffraction data for major peaks.

Sr #	2θ (degree)	Intensity (a. u)	FWHM (degree)	Crystalline size (nm)	hkl
1	33.15	619	0.23	37.92	(200)
2	32.82	313	0.17	51.76	(200)
3	32.70	285	0.063	136.56	(200)
4	32.78	165	0.15	57.64	(200)

attributes the utmost potential of electronic transport properties of the material and the effect of temperature on the thermoelectric properties [11,12]. Although much progress in achieving a high merit figure has been made in the above-mentioned cases but much work is still needed [13–22].

MgSe is a wide band gap semiconductors which is supposed to be a good candidate for electronic and optoelectronic device applications due to good electrical and elastic properties [23–25]. But the thermoelectric potential of MgSe is not investigated in the literature. Only few reports are presents on the thermoelectric properties of this materials i.e Rehman et al. investigated the thermoelectric potential of magnesium selenide thin films grown by chemical bath deposition method [44]. Therefore, there is still need to thoroughly investigate the thermoelectric properties of MgSe thin films to use this material for the fabrication of thermoelectric generators for commercial applications.

In this manuscript, we have reported some good thermoelectric parameters such as the Seebeck coefficient and power factor 6.35×10^{-8} $Wm^{-1}\,{}^{o}C^{-2}$ and 7.175×10^{-5} $V/^{\circ}C$ respectively. Such high values of the Seebeck coefficient and power factor have never been reported for MgSe, according to the best of our knowledge and available literature [26–41]. The samples under investigation were grown by thermal evaporation method using a vacuum tube furnace. A series of samples was prepared varying source to substrate distance in the tube furnace by keeping all other parameters constant during growth process.

2. Methodology

This experiment was carried out using a locally designed single-stage horizontal tube furnace (SSHTF), a simple, easy-to-operate, and cost-effective apparatus. The labeled experimental schematic diagram is given below (as Fig. 1).

- A is a Nitrogen gas cylinder
- B is a gas flow meter that also has a valve to control the flow of gas (in this experiment, we used nitrogen gas)
- C is the Vacuum gauge (Pirani gauge)
- D is the left pair of flanges made of stainless steel (SS)
- E is the Upper side heater filament
- F is the upper body of the system, which help to insulate the system and help to prevent heat dissipation into the environment
- G is the Quartz tube in which the whole experiment takes place
- H is the right pair of flange made of SS
- I is the exit control valve for gasses
- J is the vacuum pump (Rotary pump)
- K is the exhaust of the vacuum pump
- L is the lower heater filament
- M is a ceramic boat in which the material subjected to evaporation is placed
- N is the substrate holder
- O represents the substrate placed at a different distance from the source
- P is the Lower body of the experimental setup, which also helps to insulate the setup and stop heat dissipation in the environment

Before deposition the cleaning of substrates was performed to remove the impurities from the surface. Four glass substrates were washed with soap and then placed in a sonicator for 1 h. After sonication, the substrates were cleaned with acetone and dried for half an hour using a hot plate.

In 1st step, 99.9 % pure metal powder of magnesium and selenium was taken (from sigma Aldrich) in an equal ratio of 1:1. After that, grinding was performed in an agate mortar pestle to get the finer and completely mixed powder. This mixing and grinding help to get a better surface morphology of thin film on a glass substrate. In 2nd step, the physical vapor deposition method was employed using tube furnace. After that the grinding and mixing of powders, a pellet was formed and placed in a ceramic boat, and the ceramic boat was placed in a quartz tube. The position of the source material was at the center of the heating zone of the furnace. The substrate was 5, 10, 15, and 20 cm from the center. After that, 10^{-2} torr pressure was achieved using the rotary pump, and to further constrain the role of unwanted gasses like oxygen, a 100 SCCM flow of nitrogen gas was given. In the last step, the furnace temperature was set at 700°C for 1 h [42]. At 700°C, Mg and Se powder react and vaporize which forms MgSe vapor in the quartz tube and these vapors get deposited on glass substrate placed on different distance from the source. After the deposition, the furnace was cooled down to room temperature naturally under the continuous flow of nitrogen to avoid oxygen to react with MgSe vapors.

The grown samples were characterized by Raman spectroscopy (Confocal micro Raman mapping system, South Korea, the wavelength of laser used in Raman spectrometer was 633 nm, XRD (Bruker D8 advanced Germany with CuKα source of wavelength 0.154 nm), Seebeck coefficient, Hall measurement (Home made and Ecopia HMS-3000, Korea) and SEM (Emcrafts, South Korea). The temperature difference between two plates of Seebeck coefficient was achieved by heating one plate and keeping the other plate at constant temperature. The induced

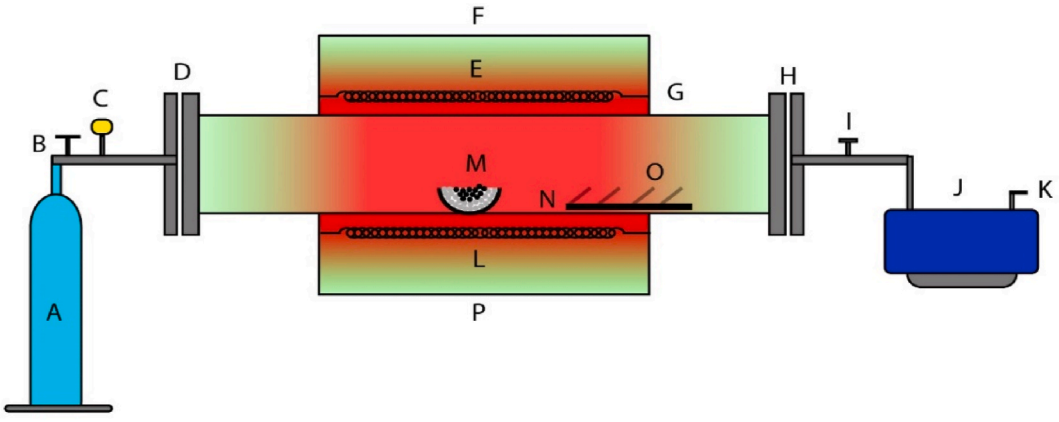

Fig. 1. The schematic diagram of the SSHTF experimental setup.

voltage at different delta temperatures was measured and graph was drawn between delta temperature and induced voltage. The slope of this graph was gives Seebeck coefficient.

3. Results and discussion

Fig. 2 demonstrates the X-ray diffraction pattern of Magnesium selenide (MgSe) thin films on a glass substrate. Two major peaks were observed at 32 and 68° which are related to Millar indices (200) and (400), respectively, according to JCPDS# 65–2922 [35]. It is further observed that as the source-to-substrate distance is increased from 5 to 20 cm, the X-ray peak intensity decreases. This degradation of crystallinity with increasing the distance between the source and substrate is due to the lack of thermal energy. As the sample moves away from the center of the furnace, the temperature gradient rises, vapor flux and decreased due to which particles don't get optimal energy to be settled in proper crystalline arrangements. There is a slight phase shift in different peaks because the stress applied by a different experimental condition caused the strain in the lattice, which shows slight fluctuations from the position [36,39].

Fig. 3 shows the effect of source-to-substrate distance on crystalline size and the FWHM in graphical interpretation to get an overview of behavior. This chart shows that as the source-to-substrate distance is increased, the crystalline size is increased up to 15 cm and then slightly decreased. The observed increase in crystalline size leads to the relation between rate of deposition, adatom mobility and surface diffusion during the growth process. At 5 cm the temperature and vapor flux were high which results in high deposition rate and surface diffusion was limited. As the distance increased at 10, and 15 cm now substrates are placed slightly lower temperature zone and have lower vapor flux, deposition rate and the overall reduced thermal energy that helps for better adatom mobility and surface diffusion. For 20 cm all the relevant parameters decreased significantly which caused less favorable condition for crystal growth so the crystallite size decreased. As the source-to-substrate distance increases, the FWHM shows a decreasing trend up to 15 cm and then shows a slight increase. The detailed of all parameters was shown in table 1.

Fig. 4 depicts the Raman spectrum of MgSe thin films grown on a glass substrate. In this pattern, one (LO) mode can be observed at 341 $cm^{-1,}$ which shows characteristic of Mg-Se bond vibration in the lattice and as the source to the substrate distance increases, the intensity of vibration decreases. This behavior showed a similar trend as demonstrated in the XRD pattern that means films are away from source have low crystallinity because of reduced thermal energy and also have low adatom mobility during deposition [43,44]. The slight peak shift is because of the reduced crystalline size can cause the confinement of the phonon which results in peak shift.

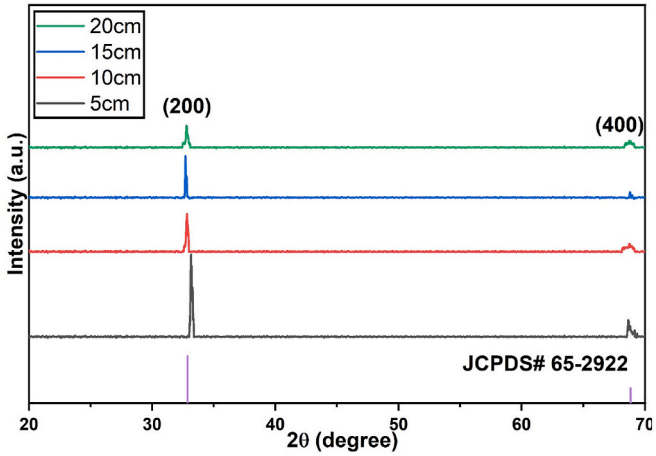

Fig. 2. The Xray diffraction pattern of Magnesium selenide.

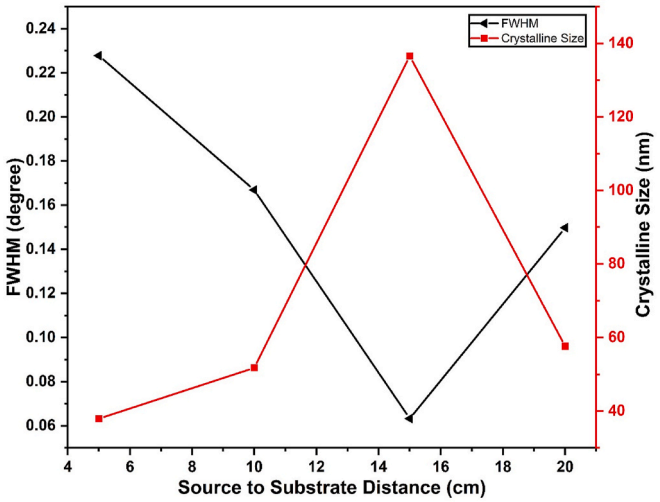

Fig. 3. The effect of source-to-substrate distance on FWHM & Crystalline size.

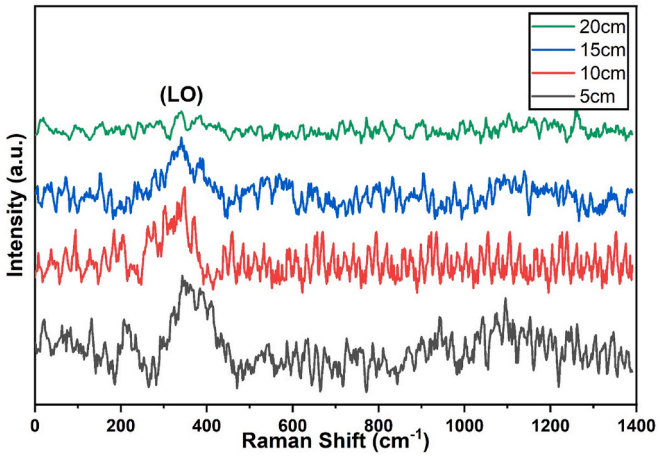

Fig. 4. The Raman spectroscopy Pattern of Magnesium selenide.

In Fig. 5 shows the Scanning electron microscope (SEM) micrographs. It can be seen that in fig (a), the surface is quite smooth and coherent, which shows the smooth surface morphology of the sample that was prepared at SSD 5 cm. In Fig (b) surface is still somehow coherent in some places, and rough patches start appearing. Fig (c) shows that the smooth surface turned slightly into a granular structure for the sample at 15 cm. In fig (d), the surface becomes vividly granular, and grains are very visible in this micrograph representing a 20 cm sample surface. This pattern is because the energy required is higher to get a smooth texture. And the surface with grains is because there is a temperature gradient, so it is evident that being far from the center and less energy transferred to the particles are responsible for this type of structure. These SEM micrographs were obtained using Scanning Electron Microscope (EMCRAFT Cube-Series).

The effect of source-to-substrate distance on the electrical conductivity/resistivity is described in Fig. 6. As the source to the substance is varied from 5 cm to 15 cm, the electrical conductivity decreases and electrical resistivity increases. The decrease in crystalline behavior (as evident in XRD data) may cause a decrease in electrical conductivity and an increase in resistivity, which controls the transfer of charge carriers, resulting in slightly lower thermal conductivity. Further verification of this argument was done by SEM as well. SEM images already demonstrated that grain boundaries play their part in increasing the electrical

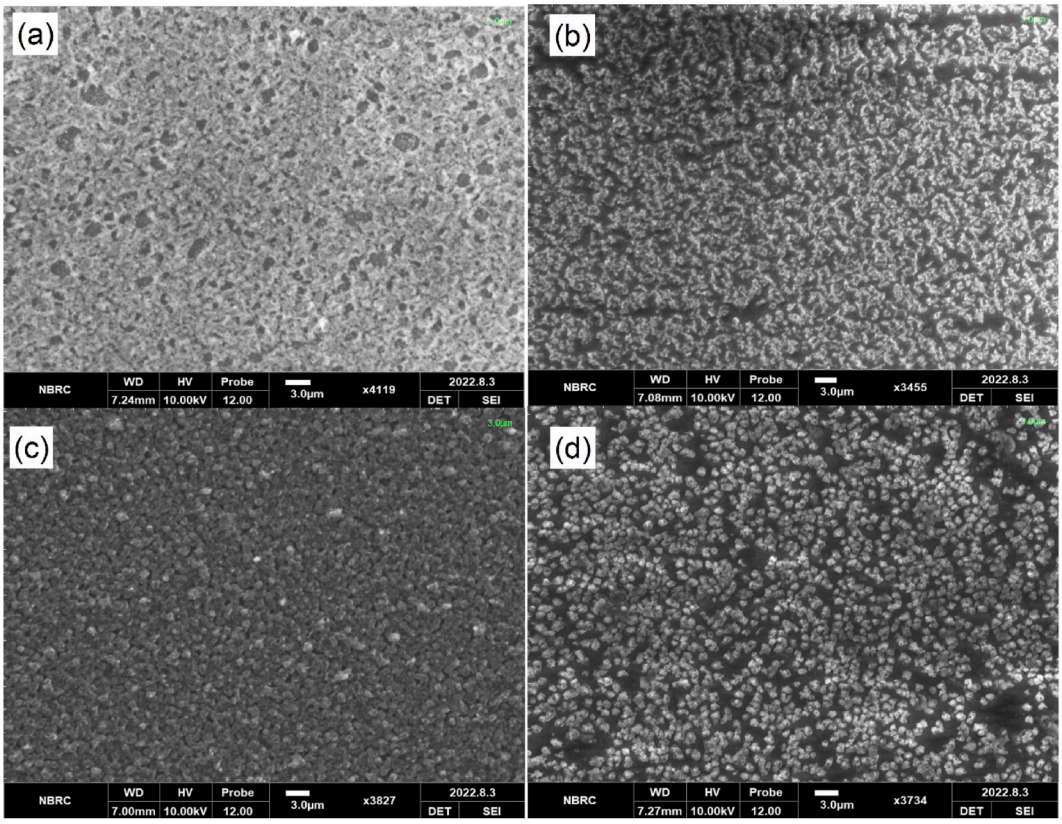

Fig. 5. The scanning electron microscope (SEM) morphological images deposited (a)5 cm, (b) 10 cm, (c) 15 cm, and (d) 20 cm.

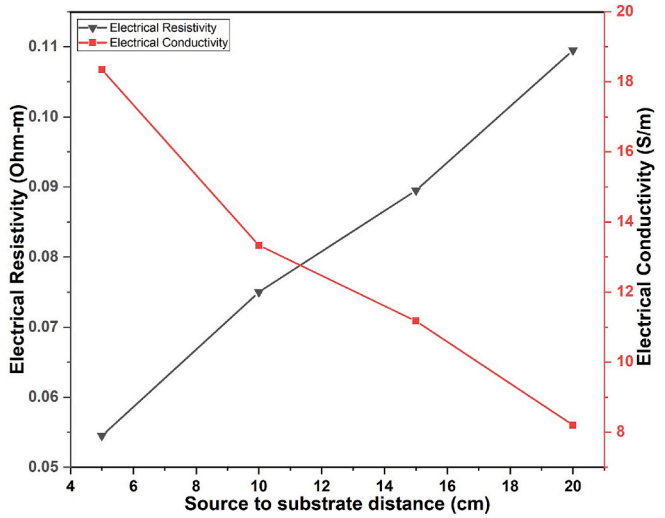

Fig. 6. The effect of source-to-substrate distance on Electrical resistivity and conductivity.

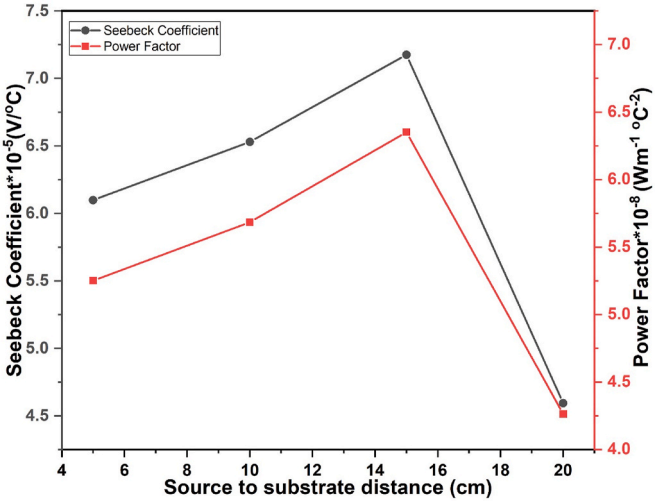

Fig. 7. The effect of the source-to-substrate distance on the Seebeck Coefficient & Power factor.

resistivity as the grain starts appearing. The grain boundaries act as barriers for the low-energy carriers at the grain boundaries, which results in the enhancement of the mobility of carriers. The high mobility of carriers simultaneously enhances the Seebeck coefficient and power factor (discussed in Fig. 7). The main understanding lies in microstructural evolution of grown thin films and how it impacts the charge carrier dynamics. The main factors which caused the high carrier mobility despite the reduced crystallinity are reduced grain boundary scattering, reduced defects, and suppressed phonon scattering. Fewer grain boundaries mean less number of obstacle for carrier transport and less scattering will be observed and similarly few defects means less traps for charge carriers. Similarly, phonon scattering will be reduced as the crystallinity will decreases which also accounts for high mobility. At 5 cm the deposition rate was high which causes more defects and more grain boundaries which results in high carrier concentration due to defect induced doping. At distance 10 and 15 cm the grain size has improved with fewer grain boundaries as compared to 5 cm which results in less trapping and scattering and better mobility of charge carriers. At 20 cm the lower thermal energy caused the smaller grain size which means more grain boundaries and more scattering of charge carriers which translates into reduced mobility of charge carriers.

Fig. 7 shows the relation between source to substrate distance with the Seebeck coefficient and power factor. We have applied the controlled temperature difference across sample to measure the electrical conductivity and Seebeck coefficient. One end of the sample was placed on heater to heat it incrementally from room temperature up to 50°C. The heater temperature was increased in 5°C–25°C. At each step we measured the induced voltage which is used to calculate Seebeck coefficient using ($-\Delta V/\Delta T$). In this graph, it can be seen that as the distance between the source and substrate varies from 5 to 15 cm, the value of the Seebeck coefficient increases and achieves the best value at 15 cm. After that, it starts decreasing because the crystallinity drops at 20 cm very much, as evident from the X-ray diffraction pattern and Raman spectrum. It can also be substantiated from the SEM micrographs that as the surface becomes more granular and more grain boundaries appear, and it starts affecting its efficiency. The value of the Seebeck coefficient and power factor has seen an abrupt decrease in the values of the Seebeck coefficient and power factor.

4. Conclusion

This article presents the synthesis of MgSe thin films using a simple and cost-effective thermal evaporation technique. Four samples were prepared on glass substrate using different source-to-substrate distances (5–20 cm). The effect of source-to-substrate distance on the structural, electrical, and thermoelectric properties was determined using XRD, Raman, and Seebeck measurements. The observed highest values for power factor and Seebeck coefficient are 6.35×10^{-8} Wm^{-1} $^{o}C^{-2}$ and 7.175×10^{-5} $V/^{\circ}C$, respectively, which were observed for a sample synthesized using substrate to source distance 15 cm. This improved performance is attributed to the balance between high carrier mobility and low carrier concentration because of improved crystallinity and large grain size. This work not only improve the understanding of MgSe thin films and also provide a base foundation for future research into efficient thermoelectric materials.

CRediT authorship contribution statement

Anas Al Tarabsheh and K. Mahmood has initiated the idea. The samples were prepared by A. Rehaman and M. Yasir Ali. Characterization of samples was done by K. Javaid and S. Ikram. A. Ali and Lamia Ben Farhat has performed the analysis. Jolly Jacob has helped in writting the manuscript.

Declaration of competing interest

The authors declare that they have no known competing financial interests or personal relationships that could have appeared to influence the work reported in this paper.

Acknowledgement

Authors acknowledge the financial of Higher Education Commission under National Research Program for Universities project number 20-16346NRPU/R&D/HEC/2021-2020.

Data availability

Data will be made available on request.

References

[1] Z. Wu, S. Zhang, Z. Liu, E. Mu, Z. Hu, Thermoelectric converter: strategies from materials to device application, Nano Energy 91 (2022) 106692.
[2] L. Pan, D. Bérardan, N. Dragoe, High thermoelectric properties of n-type AgBiSe2, J. Am. Chem. Soc. 135 (2013) 4914–4917.
[3] U. Rehman, K. Mahmood, A. Ali, A. Ashfaq, A. Rehman, M.A. un Nabi, M.I. Arshad, N. Amin, S. Ikram, S. Hussain, Optimizing the electrical transport properties of ZnSnO thin films by post growth annealing in air, Optik 204 (2020) 164148.
[4] U. ur Rehman, K. Mahmood, A. Ashfaq, A. Ali, S. Tahir, S. Ikram, A. Rehman, K. ul Sahar, W. Ahmad, N. Amin, Enhanced thermoelectric performance of hydrothermally synthesized CuFeS2 nanostructures by controlling the Cu/Fe ratio, Mater. Chem. Phys. 279 (2022) 125765.
[5] M.R. Simmons, Twilight in the Desert: the Coming Saudi Oil Shock and the World Economy, John Wiley & Son, 2006 s.
[6] L. Zheng, W. Li, S. Lin, J. Li, Z. Chen, Y. Pei, Interstitial defects improving thermoelectric SnTe in addition to band convergence, ACS Energy Lett. 2 (2017) 563–568.
[7] Z. Chen, Z. Jian, W. Li, Y. Chang, B. Ge, R. Hanus, J. Yang, Y. Chen, M. Huang, G. J. Snyder, Lattice dislocations enhancing thermoelectric PbTe in addition to band convergence, Adv. Mater. 29 (2017) 1606768.
[8] S. Roychowdhury, T. Ghosh, R. Arora, M. Samanta, L. Xie, N.K. Singh, A. Soni, J. He, U.V. Waghmare, K. Biswas, Enhanced atomic ordering leads to high thermoelectric performance in AgSbTe2, Science 371 (2021) 722–727.
[9] J.P. Heremans, V. Jovovic, E.S. Toberer, A. Saramat, K. Kurosaki, A. Charoenphakdee, S. Yamanaka, G.J. Snyder, Enhancement of thermoelectric efficiency in PbTe by distortion of the electronic density of states, Science 321 (2008) 554–557.
[10] Y. Pei, X. Shi, A. LaLonde, H. Wang, L. Chen, G.J. Snyder, Convergence of electronic bands for high performance bulk thermoelectrics, Nature 473 (2011) 66–69.
[11] W. Liu, X. Tan, K. Yin, H. Liu, X. Tang, J. Shi, Q. Zhang, C. Uher, Convergence of conduction bands as a means of enhancing thermoelectric performance of n-type Mg 2 Si 1− x Sn x solid solutions, Phys. Rev. Lett. 108 (2012) 166601.
[12] J. Dong, F.-H. Sun, H. Tang, J. Pei, H.-L. Zhuang, H.-H. Hu, B.-P. Zhang, Y. Pan, J.-F. Li, Medium-temperature thermoelectric GeTe: vacancy suppression and band structure engineering leading to high performance, Energy Environ. Sci. 12 (2019) 1396–1403.
[13] C. Hu, K. Xia, C. Fu, X. Zhao, T. Zhu, Carrier grain boundary scattering in thermoelectric materials, Energy Environ. Sci. 15 (2022) 1406–1422.
[14] Y. Pei, A.D. LaLonde, H. Wang, G.J. Snyder, Low effective mass leading to high thermoelectric performance, Energy Environ. Sci. 5 (2012) 7963–7969.
[15] C. Fu, T. Zhu, Y. Liu, H. Xie, X. Zhao, Band engineering of high performance p-type FeNbSb based half-Heusler thermoelectric materials for figure of merit zT> 1, Energy Environ. Sci. 8 (2015) 216–220.
[16] K. Imasato, S.D. Kang, G.J. Snyder, Exceptional thermoelectric performance in Mg 3 Sb 0.6 Bi 1.4 for low-grade waste heat recovery, Energy Environ. Sci. 12 (2019) 965–971.
[17] Y. Xiao, D. Wang, Y. Zhang, C. Chen, S. Zhang, K. Wang, G. Wang, S.J. Pennycook, G.J. Snyder, H. Wu, Band sharpening and band alignment enable high quality factor to enhance thermoelectric performance in n-type PbS, J. Am. Chem. Soc. 142 (2020) 4051–4060.
[18] M. Tan, Y. Deng, Y. Wang, Ordered structure and high thermoelectric properties of Bi2 (Te, Se) 3 nanowire array, Nano Energy 3 (2014) 144–151.
[19] R. Moshwan, W.-D. Liu, X.-L. Shi, Y.-P. Wang, J. Zou, Z.-G. Chen, Realizing high thermoelectric properties of SnTe via synergistic band engineering and structure engineering, Nano Energy 65 (2019) 104056.
[20] H. Cheng, X. He, Z. Fan, J. Ouyang, Flexible quasi-solid state ionogels with remarkable seebeck coefficient and high thermoelectric properties, Adv. Energy Mater. 9 (2019) 1901085.
[21] K. Mahmood, J. Jacob, A. Rehman, A. Ali, U. Rehaman, N. Amin, S. Ikram, A. Ashfaq, S. Hussain, Modulation of thermoelectric properties of Mg2GeO4 thin films by controlling the growth process, Ceram. Int. 45 (2019) 18701–18703.
[22] A. Rehman, J. Jacob, R. Zahra, K. Mahmood, A. Ali, U. Rehaman, Y. Ali, A. Ashfaq, W. Ahmed, S. Ikram, Growth of Mg2GeO4 nano-crystals on Si substrate and modulation of Seebeck coefficient by post growth annealing technique, Ceram. Int. 45 (2019) 16275–16278.
[23] M. Wei, X.L. Shi, Z.H. Zheng, F. Li, W.D. Liu, L.P. Xiang, Y.S. Xie, Y.X. Chen, J. Y. Duan, H.L. Ma, Directional thermal diffusion realizing inorganic Sb2Te3/Te hybrid thin films with high thermoelectric performance and flexibility, Adv. Funct. Mater. 32 (2022) 2207903.
[24] D.W. Ao, W.D. Liu, Z.H. Zheng, X.L. Shi, M. Wei, Y.M. Zhong, M. Li, G.X. Liang, P. Fan, Z.G. Chen, Assembly-free fabrication of high-performance flexible inorganic thin-film thermoelectric device prepared by a thermal diffusion, Adv. Energy Mater. 12 (2022) 2202731.
[25] Z.-H. Zheng, X.-L. Shi, D.-W. Ao, W.-D. Liu, M. Li, L.-Z. Kou, Y.-X. Chen, F. Li, M. Wei, G.-X. Liang, Harvesting waste heat with flexible Bi2Te3 thermoelectric thin film, Nat. Sustain. (2022) 1–12.
[26] L.D. Hicks, M.S. Dresselhaus, Effect of quantum-well structures on the thermoelectric figure of merit, Phys. Rev. B 47 (1993) 12727.
[27] J.R. Sootsman, D.Y. Chung, M.G. Kanatzidis, New and old concepts in thermoelectric materials, Angew. Chem. Int. Ed. 48 (2009) 8616–8639.
[28] J.P. Heremans, B. Wiendlocha, A.M. Chamoire, Resonant levels in bulk thermoelectric semiconductors, Energy Environ. Sci. 5 (2012) 5510–5530.
[29] H. Goldsmid, Improving the power factor and the role of impurity bands, J. Electron. Mater. 42 (2013) 1482–1489.
[30] S. Lee, K. Esfarjani, T. Luo, J. Zhou, Z. Tian, G. Chen, Resonant bonding leads to low lattice thermal conductivity, Nat. Commun. 5 (2014) 3525.
[31] W. Qiu, L. Xi, P. Wei, X. Ke, J. Yang, W. Zhang, Part-crystalline part-liquid state and rattling-like thermal damping in materials with chemical-bond hierarchy, Proc. Natl. Acad. Sci. USA 111 (2014) 15031–15035.

[32] B. Poudel, Q. Hao, Y. Ma, Y. Lan, A. Minnich, B. Yu, X. Yan, D. Wang, A. Muto, D. Vashaee, High-thermoelectric performance of nanostructured bismuth antimony telluride bulk alloys, Science 320 (2008) 634–638.
[33] X. Wang, H. Lee, Y. Lan, G. Zhu, G. Joshi, D. Wang, J. Yang, A. Muto, M. Tang, J. Klatsky, M.S. Dresselhaus, G. Chen, Z.F. Ren, Appl. Phys. Lett. 93 (2008) 193121.
[34] S. Chen, K.C. Lukas, W. Liu, C.P. Opeil, G. Chen, Z. Ren, Effect of Hf concentration on thermoelectric properties of nanostructured n-type half-heusler materials HfxZr1–xNiSn0. 99Sb0. 01, Adv. Energy Mater. 3 (2013) 1210–1214.
[35] Y.S. Sakhare, N.R. Thakare, A.U. Ubale, Influence of quantity of spray solution on the physical properties of spray-deposited nanocrystalline MgSe thin films, St-petersburg-polytechnical-university-journal-physics-and-mathematics 2 (2016) 29–40.
[36] F. Drief, A. Tadjer, D. Mesri, H. Aourag, First principles study of structural, electronic, elastic and optical properties of MgS, MgSe and MgTe, Catal. Today 89 (2004) 343–355.
[37] F.A. Sahraoui, F. Arab, S. Zerroug, L. Louail, First-principles study of structural and elastic properties of MgSe under hydrostatic pressure, Comput. Mater. Sci. 41 (2008) 538–541.
[38] G. Gokoglu, M. Durandurdu, O. Gulseren, First principles study of structural phase stability of wide-gap semiconductors MgTe, MgS and MgSe, Comput. Mater. Sci. 47 (2009).
[39] A.U. Ubale, Y. Sakhare, S. Ibrahim, M. Belkhedkar, Structural, optical and electric properties of nanocrystalline MgSe thin films deposited by chemical route using triethanolamine as a complexing agent, Solid State Sci. 23 (2013) 96–101.
[40] F. Jiang, Q. Liao, G. Fan, C. Xiong, X. Peng, C. Pan, N. Liu, MOCVD growth of MgSe thin films on GaAs substrates, J. Cryst. Growth 183 (1998) 289–293.
[41] J. Bettini, M. de Carvalho, M. Cotta, M. Pudenzi, N. Frateschi, A. Silva, E. Baba Ali, J.C. Bernede, P. Le Ray, Vanadium transition metal oxide" lms obtained by annealing under room atmo-sphere of metal layers sequentially depos-ited 208 (2000) 471, J. Cryst. Growth 208 (2000) 820.
[42] A. Rehman, A. Ali, S. Ikram, M. Amami, K. Mahmood, Characterization of polycrystalline SnSe2 thin films for thermoelectric applications grown by single-stage horizontal tube furnace (SSHTF), Opt. Mater. 133 (2022) 112797.
[43] D. Huang, C. Jin, D. Wang, X. Liu, J. Wang, X. Wang, Crystal structure and Raman scattering in Zn1− x Mg x Se alloys, Appl. Phys. Lett. 67 (1995) 3611–3613.
[44] A. Rehman, A. Ali, S. Ikram, K. Mahmood, A. Al, Tarabsheh Emerging pathways in thermoelectric: chemical bath deposition of magnesium selenide thin films for sustainable energy harvesting, Ceram. Int. 50 (11) (2024) 20758–20763.